RSC Advances

RSC Publishing

PAPER

View Article Online
View Journal | View Issue

Polyurethane–poly(2-hydroxyethyl methacrylate) semi-IPN–nanooxide composites

Cite this: *RSC Advances*, 2013, **3**, 14560

Vladimir A. Bershtein,[a] Vladimir M. Gun'ko,*[b] Lyudmila V. Karabanova,[c] Tatiana E. Sukhanova,[d] Pavel N. Yakushev,[a] Larisa M. Egorova,[a] Anna A. Turova,[b] Vladimir I. Zarko,[b] Eugene M. Pakhlov,[b] Milana E. Vylegzhanina[d] and Sergey V. Mikhalovsky[ef]

Received 21st January 2013,
Accepted 30th May 2013

DOI: 10.1039/c3ra40295a

www.rsc.org/advances

Two sets of hybrid polyurethane–poly(2-hydroxyethyl methacrylate) semi-interpenetrating polymer network–nanooxide composites with 0.25 or 3 wt% nanosilica or nanoalumina functionalised with OH, NH_2 or $CH{=}CH_2$ groups were prepared. A combination of atomic force microscopy, infrared spectroscopy, thermally stimulated depolarisation current measurement, differential scanning calorimetry and creep rate spectroscopy analysis of the nanostructure and properties of the composites was performed. The pronounced dynamic heterogeneity and the strong impact of oxide additives, basically suppression of the dynamics and temperature-dependent increasing modulus of elasticity, were observed. The effects correlated with either interfacial interactions (for silica) or the nanostructure (for alumina). A low oxide content strongly affected the matrix due to the formation of an unusual cross-linked, *via* double covalent hybridisation of three components, structure of the nanocomposites.

Introduction

Polymer composites containing small amounts of nanofiller additives have attracted great attention in industry, medicine and scientific research because a considerable enhancement of the polymer characteristics may be attained in the composites. Due to an exceptionally large polymer–nanoparticle interfacial area, nanocomposites are considered to be model systems to study the dynamics of polymers under nanoconfinement/constraining conditions. Most studies have been focused on polymer nanocomposites with 2D silicate nanolayers, oxide nanoparticles and other systems,[1,2] as well as 1D carbon nanotubes (CNTs) or other 2D or 3D nanocarbons.[3,4] The significance of factors such as good nanofiller dispersion in a matrix, high aspect (*e.g.*, length-to-diameter for CNTs) ratio, and functionalisation of a nanofiller surface for improving nanofiller dispersion and its reaction with a polymer, to provide strong interfacial bonding, has been typically emphasised. Considerable attention has also been paid to hybrid polymer–3D oxide nanocomposites, especially with silica nanoclusters formed in a matrix *via* a sol–gel process.[5–10] Some nanocomposites with 3D fumed silica nanoparticles (NPs)[11,12] have also been studied. Less attention has been paid to polymer–alumina nanocomposites.[13] Peculiar dynamics in polymer nanocomposites have been observed in a number of studies (see, *e.g.*, a review[2]). A linear polymer matrix is considered to be entirely confined in a nanovolume, and the enhancement of nanocomposite properties is expected if an average interparticle distance, L, is close to or smaller than the size of the unperturbed macromolecular random coils (radius of gyration r_g is typically of the order of 10 nm for many polymers). According to calculations,[4] the substantial impact of 3D particles of $\sim$10 nm in size on the dynamics and properties of a polymer matrix may be expected when their volume content is not less than 10%. In reality, anomalies in the glass transition dynamics have been observed, *e.g.*, at a silica content of 10 to 50 wt% in nanocomposites.[6,8,10,11] Recently we found[14,15] that monomolecular polymer layers adsorbed at a silica surface are characterised by multi-modal dynamics within the glass transition range ΔT_g extending from 80 to 230 °C, with the apparent activation energy varying from 80 to 560 kJ mol^{-1}. Meanwhile, we revealed that small amounts of additives of 3D nanoparticles (*e.g.*, 0.25 wt% only) may strongly affect the glass transition dynamics and elastic properties of polymer matrices. This was shown for 3D nanodiamond containing composites based on polyurethane–poly(2-hydroxyethyl methacrylate) (PU–PHEMA) semi-interpenetrating polymer networks (semi-IPNs).[16] This result was treated in the framework of ''double hybridisation''

[a]*Ioffe Physical-Technical Institute, RAS, 194021 St.-Petersburg, Russia. E-mail: vbersht.polmater@mail.ioffe.ru*
[b]*Chuiko Institute of Surface Chemistry, 17 General Naumov Str., Kiev, Ukraine. E-mail: vlad.gunko@ukr.net; Fax: 38044 4243567; Tel: 38044 4229627*
[c]*Institute of Macromolecular Chemistry, NASU, Kyiv 02660, Ukraine. E-mail: lyudmyla_karaban@ukr.net*
[d]*Institute of Macromolecular Compounds, RAS, St.-Petersburg 199004, Russia. E-mail: xelmic@imc.macro.ru*
[e]*School of Pharmacy & Biomolecular Sciences, University of Brighton, Brighton BN2 4GJ, U.K.. E-mail: s.mikhalovsky@brighton.ac.uk*
[f]*School of Engineering, Nazarbayev University, 53 Kabanbay Batyr Ave., Astana 010000, Kazakhstan*

between the material components resulting in the formation of an unusual cross-linked structure. A similar effect was observed also in the preliminary data obtained for the PU–PHEMA/nanosilica composites.[17] PU–PHEMA semi-IPNs are of great interest as biomedical and damping materials. Polyurethane materials are extensively used in applications involving contact with blood and organ and tissue engineering. Although PUs are relatively biocompatible materials,[18] they are also known to be prone to biodegradation,[19] stress induced degradation,[20] and surface cracking.[21] The creation of IPNs or semi-IPNs is one of the most powerful approaches to improve PU biocompatibility, mechanical properties and resistance to degradation. PHEMA is well known as a polymer with good biocompatibility but with unstable properties, due to its high hygroscopicity. Semi-IPNs create an opportunity to synthesise PU–PHEMA based composites that retain the biocompatibility of PHEMA and acquire better stability and mechanical properties due to the PU component. In our previous publications, semi-IPNs based on PU and PHEMA were synthesised[22] and studied using small angle X-ray scattering (SAXS),[23] thermodynamic miscibility analysis, dynamic mechanical analysis (DMA),[22] dielectric relaxation spectrometry (DRS),[24] differential scanning calorimetry (DSC) and laser-interferometric creep rate spectroscopy (CRS) measurements.[25] The SAXS study showed that the semi-IPNs were biphasic systems with incomplete phase separation and a nanoheterogeneous structure with characteristic quasi-periodicities of 6–9 and 22–27 nm as a consequence of spinodal decomposition.[23] The DMA analysis of the semi-IPNs showed two very broad mechanical loss peaks located between −55 and 50 °C and between 50 and 180 °C associated with PU and PHEMA glass transitions, respectively.[22] The discrete CRS analysis of the glass transition dynamics in a series of the PU–PHEMA semi-IPNs with systematically varied compositions clarified the origin of the extraordinarily broad PU and PHEMA glass transitions.[25] The complicated creep rate spectra of the semi-IPNs consisted of a few partly overlapping peaks and indicated the presence of several segmental dynamics modes, *i.e.*, the pronounced dynamic heterogeneity within each glass transition range. In the present work, we prepared and studied nanocomposites of potential biomedical and technical significance based on the hybrid PU–PHEMA network filled by a small amount of 3D silica or alumina NPs unmodified and modified by different surface functionalities. The goal of this study was to trace the impact of the NP type, dispersion degree, and surface modification, as well as the character of the interfacial interactions, on the dynamic and elastic properties of the composites.

Experimental

Materials

The hybrid PU–PHEMA semi-IPN materials were prepared with a polyurethane (PU) network and linear poly(2-hydroxyethyl methacrylate) (PHEMA) with a PU : PHEMA weight ratio of 83 : 17. First, the PU network was synthesised using a two-step method, as described previously,[22] using the adduct of trimethylol propane (TMP, Merck), toluylenediisocyanate (TDI, Bayer), and poly(oxypropylene) glycol (PPG, Bayer) with M_w = 2000 g mol^{-1}. The PU film obtained was swollen with freshly distilled 2-hydroxyethyl methacrylate (HEMA) containing 2% photoinitiator Irgacure 651, and then photopolymerisation of this monomer was carried out for 2 h using UV irradiation at λ = 340 nm. The kinetics of swelling has been previously investigated,[22] and a defined time (25 min) of PU film swelling was used to prepare the semi-IPN. The photopolymerisation of HEMA in the PU matrix was performed in a set-up consisting of two quartz glasses. To prepare the nanocomposites, 0.25 or 3 wt% of silica or alumina NPs were introduced into the matrix at the PU synthesis stage. For mixing nanooxides with the initial reagents and allowing for better dispersion, sonication by a tip sonicator was performed at 20 °C for 5 min. The prepared neat semi-IPN and nanocomposite films of 1 mm in thickness were post-cured at 100 °C for 2 h and then were held at 80 °C and 10^{-5} Pa for 36 h, to reach a constant weight.

Fumed silica A-300 (99.87% purity) and alumina (99.5% purity) NPs[26] (pilot plant of the Chuiko Institute of Surface Chemistry, Kalush, Ukraine) were heated before the composite synthesis at 450 °C for 4 h to remove residual HCl and other adsorbed compounds. The specific surface area of NPs estimated using the low-temperature nitrogen adsorption (LTNA) technique (Micromeritics ASAP 2405N adsorption analyser, 77.4 K) and the standard BET method, was S_{BET} = 295 m^2 g^{-1} and 89 m^2 g^{-1} for silica and alumina NPs, respectively. The average NP diameters were 9 nm (silica) and 25 nm (alumina) (Fig. 1a). The NP diameters in the dispersions were estimated from the LTNA adsorption/desorption isotherms using a self-consistent regularisation procedure applied to pair integral equations for pore (voids between spherical particles) and nanoparticle size distributions.[27] Fig. 1a shows that the primary NPs had a relatively narrow size distribution for silica (5–17 nm) and a broader size distribution for alumina (12–47 nm).

Oxide NPs were used with three different surface states. First, the initial silica and alumina had surface hydroxyls (''–OH cover''). Second, functionalisation was carried out by 3-aminopropylmethylsilyl groups (APMS, ''–NH_2 cover'') or 3-methacryloylpropylsilyl groups (MAPS, ''–CH=CH_2 cover''). It should be noted that native silica is characterised with a higher hydroxylation degree than native alumina.[26,28]

Functionalisation of NPs by 3-aminopropylmethyl-diethoxysilane (APMDES) was carried out in toluene. The reaction mixture was stirred at 100 °C for 10 h, the solid residue was filtrated, washed by toluene to remove excess APMDES, and then dried at 60 °C for 5 h. The content of grafted silane (by chemical analysis) corresponded to the substitution of ~40 and 30% of the surface hydroxyls by APMDES for silica and alumina NPs, respectively. Complete functionalisation of NPs by 3-methacryloyloxypropyl trimethoxysilane (MAPTMS), which was added in amounts corresponding to the surface hydroxyl content and provided complete substitution of them, was carried out in a glass reactor upon mixing at 700 rpm and 150 °C for 1 h.[12d] Then the gas-phase products were removed

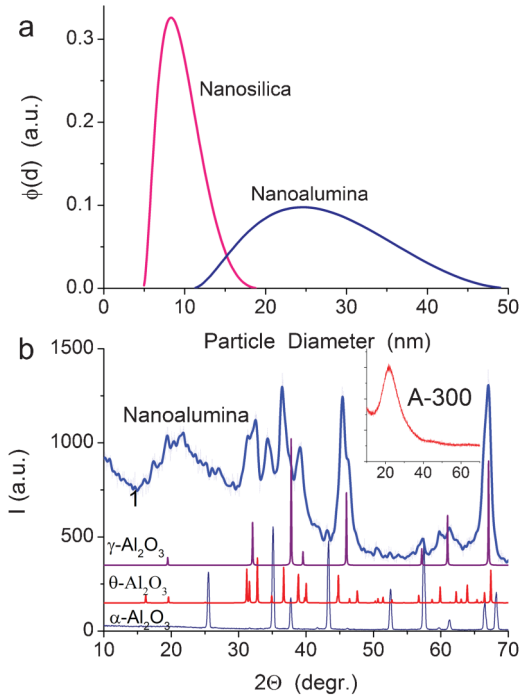

Fig. 1 (a) Size distributions of individual fumed alumina and silica NPs as estimated from the low-temperature nitrogen adsorption data;[15] and (b) X-ray diffraction patterns for nanoalumina compared to those for crystalline α-Al_2O_3, θ-Al_2O_3 and γ-Al_2O_3, and for amorphous nanosilica (insert).

during heating in air at 150 °C for 1 h. The content of the grafted silane (FTIR spectroscopy control) corresponded to practically the entire substitution of the NP surface hydroxyls by the 3-methacryloylpropylsilyl groups.

Characterisation methods

X-ray diffraction (XRD) analysis of fumed NPs showed a totally amorphous character of silica (inset in Fig. 1b), whereas nanoalumina corresponded to a mixture of crystalline γ and θ phases and an amorphous phase (Fig. 1b).

The morphology of the nanocomposite films, including the dispersion quality of the NPs in the polymer matrix, was examined by AFM using a Nanotop NT-206 instrument (Microtestmashiny, Belarus) in contact mode or in tapping mode.

A Perkin-Elmer DSC-2 apparatus was used to determine the PHEMA glass transition temperatures, T_g, at the half-height of a heat capacity step ΔC_p, and the transition width $\Delta T_g = T_g'' - T_g'$ where T_g' and T_g'' are the temperatures of the transition onset and completion, respectively. Second scans were taken for all compositions to exclude the endothermic side effect of water desorption. The measurements were performed under a nitrogen atmosphere at a heating rate of 20 °C min^{-1} over a temperature range from −20 to 197 °C after cooling from 197 to −20 °C at a rate of 320 °C min^{-1}. Amorphous quartz was used as a reference sample.

High-resolution laser-interferometric creep rate spectroscopy (CRS) was used to analyse the segmental dynamics and its heterogeneity over the 20–160 °C range covering the PHEMA glass transition range. The CRS method has been described in detail elsewhere.[29] CRS precisely measures creep rates at a constant low stress, much less than the yield stress, as a function of temperature (CR spectrum). The laser interferometer based on the Doppler effect was used for this purpose. The time evolution of deformation was registered as a sequence of low-frequency beats in an interferogram whose beat frequency (v) yields a creep rate:

$$\dot{\varepsilon} = \lambda v/2I_0 \quad (1)$$

where λ (632 nm here) is the laser wavelength, and I_0 is the initial length of the working part of a sample.

The CR spectra were measured at the tensile stress of 0.3 MPa on the basis of a deformation increment of less than 1%. A stress was chosen in the preliminary experiments as capable of inducing sufficient creep rates to be measured, while also maintaining a high spectral resolution and preventing premature rupture of a sample. Under such experimental conditions, the creep is predominantly associated with local shear strains (''microplasticity''), and its rate decreases as the creep process proceeds. Therefore, besides the stress, time t = 10 s from the moment of loading to the onset of measurement was kept constant while measuring creep rates at different temperatures. A sample was heated at a rate of 1 °C min^{-1}. The loading of a sample, the recording of an interferogram, and unloading were performed every 5 °C of heating. The instrument errors in measuring creep rates did not exceed ±1% but scattering in the CR peak height and temperature values may be as much as ±20% and ±3–5 °C, respectively, during the measurement of identical samples. Film samples with 1 × 5 mm^2 cross-sections and 5 cm in length were used. The correlative frequency of the CRS experiments was $v_{corr} \approx 10^{-3}$–10^{-2} Hz.

Besides the CR spectra, the modulus of elasticity E *versus* temperature T was measured using the laser interferometer. The E values were determined from the values of deformation ε measured after 1–2 s standing under the load by the formula:

$$\varepsilon = \lambda n/2I_0 \quad (2)$$

where n is the number of oscillations in an interferogram.

The creep rate ($\dot{\varepsilon}$) can be written as a function of applied stress (σ) and temperature using a simplified equation of the Arrhenius type assuming an activation character of the studied process without strong cooperative effects:

$$\ln\dot{\varepsilon} = A - E_a/R_gT \quad (3)$$

where A is a constant dependent on σ and other parameters but independent of temperature in a certain range, and R_g is the gas constant.

Infrared (IR) spectra were recorded using a Specord M80 (Carl Zeiss, Germany) spectrophotometer over the 4000–300 cm^{-1} range. The polymer and composite samples were cooled with liquid nitrogen and broken down to a powder state and then dried at 80 °C for 2 h. A powder sample (2–5 mg) was stirred with dry KBr (Merck, spectroscopy grade) as 1 : 50 (w/w)

using a microbreaker (100 Hz), and was then pressed (8000 bar) into a thin transparent platelet.

Thermally stimulated depolarisation current (TSDC) spectra were recorded over the temperature range from −185 to 175 °C (for some composites the temperature range was narrower) covering the regions of polymer glass transitions and sub-T_g relaxations. The tablets (diameter 30 mm, thickness ~1 mm) were polarised by the electrostatic field at the intensity $F_p \approx (2–3) \times 10^5$ V m^{-1} at 260 K, then cooled to 90 K with the field still applied and heated without the field to 265–270 K at a heating rate β = 0.05 K s^{-1}. The current (I) evolving due to sample depolarisation was recorded by an electrometer over the 10^{-15}–10^{-7} A range. Relative mean errors were $\delta_I = \pm 5\%$ (TSDC), $\delta_T = \pm 2$ K (temperature), and $\delta_\beta = \pm 5\%$ (temperature change rate).[30]

Results and discussion

Morphology of the composites

Fig. 2a and 2b show AFM images of a surface of an 83PU–17PHEMA nanocomposite film with 3 wt% MAPS–A-300 (as a representative sample). Three kinds of NP dispersion states could be discerned in this case: (i) individual particles or their small aggregates (discernible black "points") of 20–40 nm in size; (ii) particle aggregates of ~100 nm in size, and (iii) rather sparse aggregates of 200–400 nm in size. Generally, all these dispersion states were revealed irrespective of the type of functional groups at the nanosilica surface.

Of importance, no substantial changes in silica dispersion were revealed after functionalising its surface. This is an unexpected result, at first thought, since functionalisation is typically considered as a route to improve the nanofiller dispersion. This result may be understood as follows. Silica NPs were introduced into the reaction mixture at the stage of PU synthesis in the presence of isocyanate groups, which are very active chemically with –OH and APMS groups at both untreated and APMS functionalised silica surfaces. Therefore it is natural to expect the formation of similar nanostructures in the nanocomposites. Functionalisation of silica with MAPS groups, which are not capable of reacting with the components of the PU-forming reaction mixture (before introducing HEMA), could, in principle, even enhance silica aggregation to some extent. However, similar composite nanostructures were observed, in fact, in all three cases. Of significance, this allowed us to estimate the impact of changes in the silica-matrix interfacial interactions on the glass transitions dynamics in these nanocomposites.

Different and more complicated nano- and microstructures were revealed by AFM for the nanocomposite film samples with 0.25 and 3 wt% alumina NPs. Additionally, AFM height images of the free film surface and the surface which was in contact with a substrate had different morphology.

Free surface of samples with 0.25 wt% as-prepared alumina NPs exhibited a relatively smooth morphology. Individual particles of 20–50 nm in size were seen in the matrix with only a few aggregates of 200–500 nm in size. On the surface which was in contact with the substrate sporadically distributed

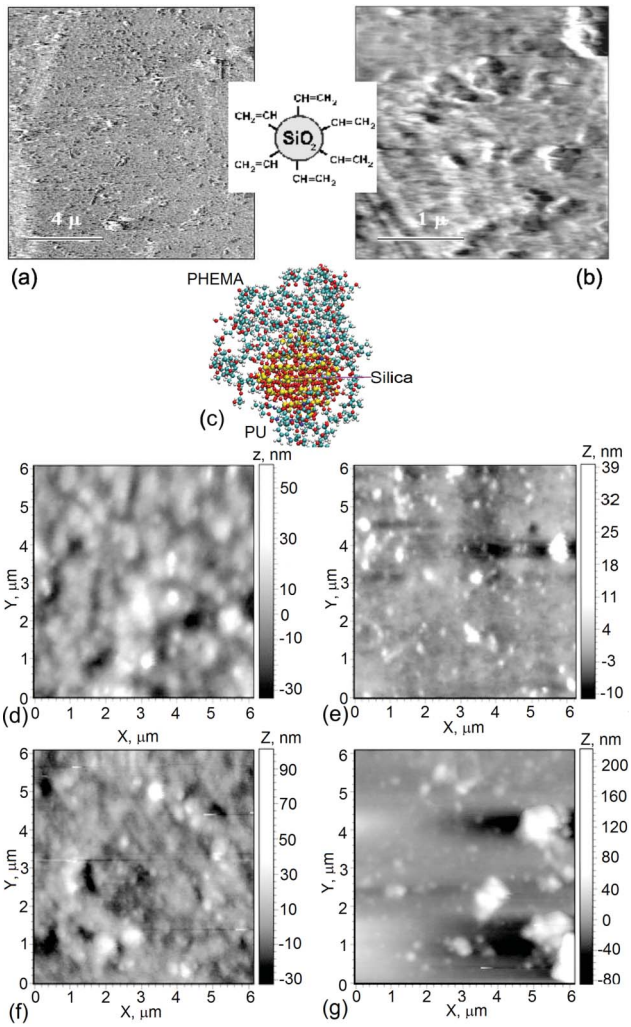

Fig. 2 Deflection AFM images, obtained in contact mode, of 83PU–17PHEMA-based nanocomposite film surface with (a, b) 3 wt% MAPS–A-300, (c) molecular model of a silica nanoparticle covered by PU–PHEMA; and 6 × 6 μm images of polymers with (d, e) 0.25 wt% or (f, g) 3 wt% MAPS-functionalised alumina with (d, f) free surface and (e, g) surface contacted with a substrate.

pores of 100–200 nm in diameter were present. Individual NPs (20–50 nm) and their large agglomerates of 0.5 to 2 μm in size could be seen. Introducing NH_2 or $CH{=}CH_2$ functionalised alumina NPs into the polymer matrix drastically changed the morphology of the nanocomposites. Fig. 2d–2g show that the surface modification of NPs leads to particle agglomeration and the formation of a more loosened surface morphology consisting of domains from 0.1 to 1 μm or 200 to 400 nm in size, with a lot of voids and channels between the domains. It is probable that these domains are the NP aggregates with a surrounding polymer coating or the loosened polymer matrix itself because some separate NPs between domains are observed. The surface which was in contact with a substrate is more smooth, with separate particles of 20–50 nm in size, and aggregates of 300 to 600 nm in size, and with pores. A different morphology is observed for the samples with 3 wt% alumina NPs. The surface of a sample with bare NPs displays mainly aggregates composed of tens to hundreds of NPs

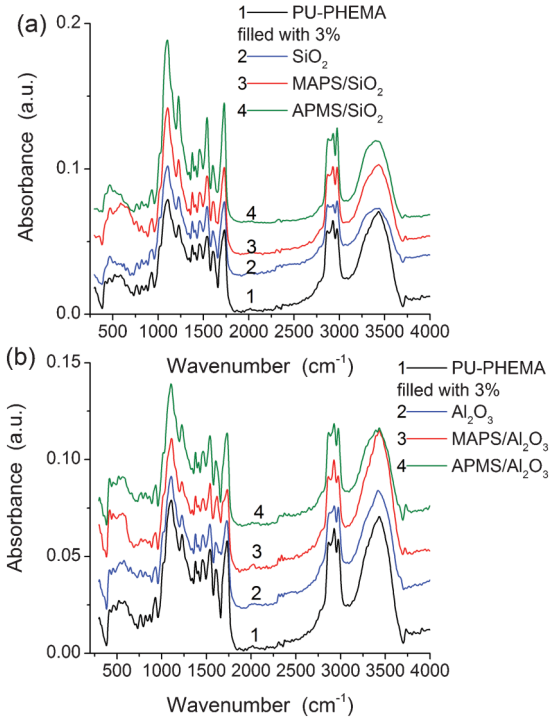

Fig. 3 Infrared spectra of 83PU-17PHEMA alone and filled with 3 wt.% of (a) unmodified or modified silica and (b) unmodified or modified alumina.

(resembling a "bunch of grapes" morphology). The bottom surface is smooth, with particle agglomerates from 200 to 500 nm in size. Samples with functionalised NPs contain not only the NP aggregates of hundreds of nanometers in size but also less dense structures, highly porous on both sides. Thus, AFM images showed different kinds of film morphology and alumina NPs agglomeration as well as various types of porosity and voids in the films.

There are several factors preventing a uniform NP (especially alumina) distribution in the polymer matrix. Fumed silica and alumina NPs are totally aggregated in the initial state.[26] Due to a highly hydrophilic surface, the NPs also tend to remain in aggregates in nonpolar or weakly polar organic media. Stronger total hydroxylation of silica NPs than alumina[26,28] and an inevitable fast isocyanate-hydroxyl reaction promote, obviously, decreasing silica NP aggregation, although the disaggregation of NPs is incomplete. Nevertheless, for the composites with silica or 0.25 wt% of unmodified alumina, the NPs are relatively uniformly distributed in the polymer matrix and form comparatively dense morphological structures.

The IR spectra (Fig. 3) show that the introduction of 3 wt% of different oxide nanofillers has a weak influence on the chemical structure of the polymer matrix since all the spectra are practically identical. This result can be explained by a relatively low content of the fillers. The filled polymer films were transparent. This and also a low baseline in the IR spectra, *i.e.* low scattering effects, also indicated the relatively satisfactory distribution of NPs in the polymer matrix. Thus, the IR spectra show that the stretching and deformation vibrations of the bonds in the polymer matrix weakly depend on the presence of NPs. However, the dynamics of such structures as atomic groups, monomer units, and segments of polymer molecules, especially interfacial dynamics, could be changed substantially due to interactions of the macromolecules with the NPs. These aspects could be analysed using the TSDC, DSC and CRS methods.

TSDC data

The total uniformity of the composites studied with respect to the filler distribution in the polymer matrix could not be attained but the value of the interfacial area between the polymer matrix and nanoparticles was relatively large ($\sim$90 m^2 g^{-1} Al_2O_3 and $\sim$300 m^2 g^{-1} SiO_2). This is due to the following reason: NPs aggregates and agglomerates (observed in powders alone or aqueous suspensions[26,30]) can be decomposed in the polymer matrix because the interactions of NPs with monomers and the polymer matrix can be stronger than with neighbouring NPs in aggregates and agglomerates. Enhanced interfacial interactions in the nanocomposites can obviously change the matrix dynamics and, as a consequence, the physicochemical properties of the composites. This was confirmed by the TSDC spectra (recorded in a broad temperature range) for the PU–PHEMA and by the DSC/CRS data for the temperature region of the PHEMA glass transition (*vide infra*).

There are several types of secondary, sub-T_g (δ, γ, and β) relaxations and a primary glass (α) transition in glass-forming materials[30,31] appearing with increasing temperature. In particular, the γ-relaxation is faster (typically occurring on a time scale on the order of picoseconds at room temperature) than the β-relaxation and occurs at lower temperatures in isochronal (constant frequency) experiments.[32] In polymers, low-angle rotations of small structural elements, such as polar atomic groups on the scale of two to three monomer units[33] or polar side groups,[29] are responsible for the γ-relaxation. Larger moving units, such as polymer Kuhn segments, give the β-relaxation (quasi-independent segmental motions locally in the increased free volume places[29,33,34]) and the main cooperative glass transition (α-relaxation). Additionally, interfacial Maxwell–Wagner–Sillars (MWS) and conductivity (CR) relaxations as well as the through conductivity (TC, *i.e.*, direct current relaxation) are typically observed in the TSDC thermograms at higher temperatures.[30]

Fig. 4a shows the TSDC thermograms recorded for PU, PHEMA and neat PU–PHEMA networks and Fig. 4b gives the spectra for PU–PHEMA based nanocomposites.

Neat PU and PU–PHEMA semi-IPNs (Fig. 4a) distinctly demonstrate several types of relaxations within the PU component, γ at about −125 °C, β at approx. −60 °C, and an α-relaxation peak extending from approx. −30 to 20 °C, with the maximum at −10 to 0 °C. Additionally, the TSD current observed at $T > 20$ °C could be assigned to MWS, CR and TC in the case of PU (curve 1). Secondary relaxations for dry neat PHEMA are observed at −90 °C and −150 °C, respectively, whereas an α (glass) transition is expected at much higher temperatures (around 100 °C, see DSC and CRS data below). The latter may appear in TSDC thermograms overlapping well with MWS, CR and TC for the PU component. In reality, the increase in the TSD current at high temperatures in a

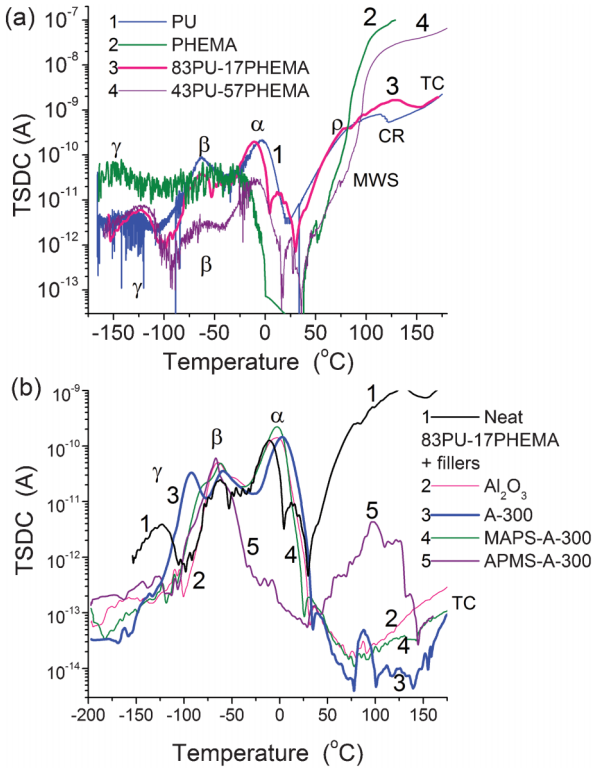

Fig. 4 TSDC thermograms of (a) pure polymers and (b) 83PU–17PHEMA alone (curve 1) and filled with 3 wt% of alumina (2) or unmodified (3) or modified silica A-300 (curves 4 and 5).

sequence of samples PU, 83PU–17PHEMA, 43PU–57PHEMA, PHEMA (Fig. 4a) may presumably be assigned to an increasing contribution from the PHEMA glass transition.

Fig. 4b shows that the presence of NPs changes the PU–PHEMA thermogram over the whole temperature range under study but the strongest effects are observed in the region of high temperature relaxations (MWS, CR and TC) at $T > 20$ °C and for the nanocomposite with APMS–A-300 in the range of PU α-relaxation (curve 5). Of importance, the impact being observed depends not only on the NP type but also on the situation at the interfaces; *i.e.*, on the NP surface coverage (prevailing functional groups) indicating the key role of interfacial dynamics. At temperatures below 20 °C, different effects of suppression of the dynamics in the PU component by 3% of NPs may be seen. In particular, there is some suppression or displacement (from −125 to −95 °C) of the γ relaxation peak, small changes in the location and intensity of β-relaxation, and decrease and displacement of the PU glass transition (α-peak) by a few degrees towards higher temperatures for composites in comparison with that in the neat polymer matrix. The anomalously strong suppression of the PU glass transition by AMPS–A-300 NPs (curve 5) is observed, obviously, due to a rapid reaction of amine groups (AMPS) with isocyanate groups in the process of forming the PU network providing the covalent interactions of PU with NPs and constrained dynamics effects.[2,29] On the contrary, the latter effect is negligibly small in the cases of more aggregated alumina NPs (curve 2) or MAPS–A-300 (curve 4) because of the absence of covalent bonding between MAPS and isocyanate groups.

Finally, of special interest is the strong impact of NPs on the TSD current at 20–175 °C (Fig. 4b): a decrease in the intensity of the TSDC relaxations by 3–5 orders of magnitude for composites in comparison with that for the neat polymer matrix is observed (curves 2–4). The effect is less pronounced for the nanocomposite with AMPS–A-300 NPs (curve 5). This result may be interpreted in two ways. First, it may be associated with enhanced proton mobility and could be explained by faster discharging of polarised structures due to increased amounts of water bound to nanooxide particles. Moreover, the less pronounced impact of AMPS–A-300 NPs for relaxation in this temperature region (curve 5) is explained by weaker interactions at the PHEMA–nanooxide interfaces in this composite since the NP amine groups are not capable of forming covalent bonds with PHEMA. The assumption about constraining dynamics in the PHEMA glass transition in the nanocomposites is in accordance with the DSC and CRS experimental data given below.

Fig. 5 shows DSC curves to characterise the PHEMA glass transition in the dehydrated 83PU–17PHEMA network and related nanocomposites.

Unlike the "usual", one-stage transition at T_g = 85 °C and transition width ΔT_g = 37 °C for the neat PHEMA,[16a] a strongly broadened, two-step PHEMA glass transition extending from 33 to 147 °C, at T_{g1} = 77 °C and T_{g2} = 137 °C (curve 1), was observed for the neat 83PU–17PHEMA network. This supposes the pronounced dynamic heterogeneity within its glass transition range (*vide infra*). As was evidenced by the IR spectra,[25] the second, higher-temperature ΔC_p step was caused by covalent hybridisation of a part of the PHEMA segments (hydroxyls) with the PU network junctions (residual isocyanate groups). Impeded dynamics in the "attached" PHEMA segments could be caused by an increasing motion event scale making conformational transitions more difficult. Thus, this PU–PHEMA network could be considered as a hybrid semi-IPN one.

Fig. 5 depicts a substantial and quite different impact of the added oxide NPs on the characteristics of the PHEMA glass transition in the 83PU–17PHEMA network. It depends on the type of NPs, their content and the type of functionalisation ("surface cover"), *i.e.*, on the interfacial dynamics. The following changes in the course of the DSC curves are observed: the total disappearance of the second ΔC_p step; a sharp narrowing of the glass transition range; a large increase in T_g and especially the T_g' values, and a change in the ΔC_p values in the opposite directions. The disappearance of the higher temperature ΔC_p step in some of the DSC curves corresponds, obviously, to suppression of the mobility of the PHEMA segments covalently anchored to the network constituents or located very close to the anchoring points.

For the silica-containing nanocomposites (Fig. 5a), the most impressive DSC result is the quite different impact of 0.25 wt% NPs on the PHEMA glass transition. This distinctly demonstrates the connection between dynamics and the type of functional groups at the NP surface, *i.e.*, with the character of interfacial interactions (curves 2, 4, and 6). In reality, the –OH and APMS coverage could provide only hydrogen bonding of

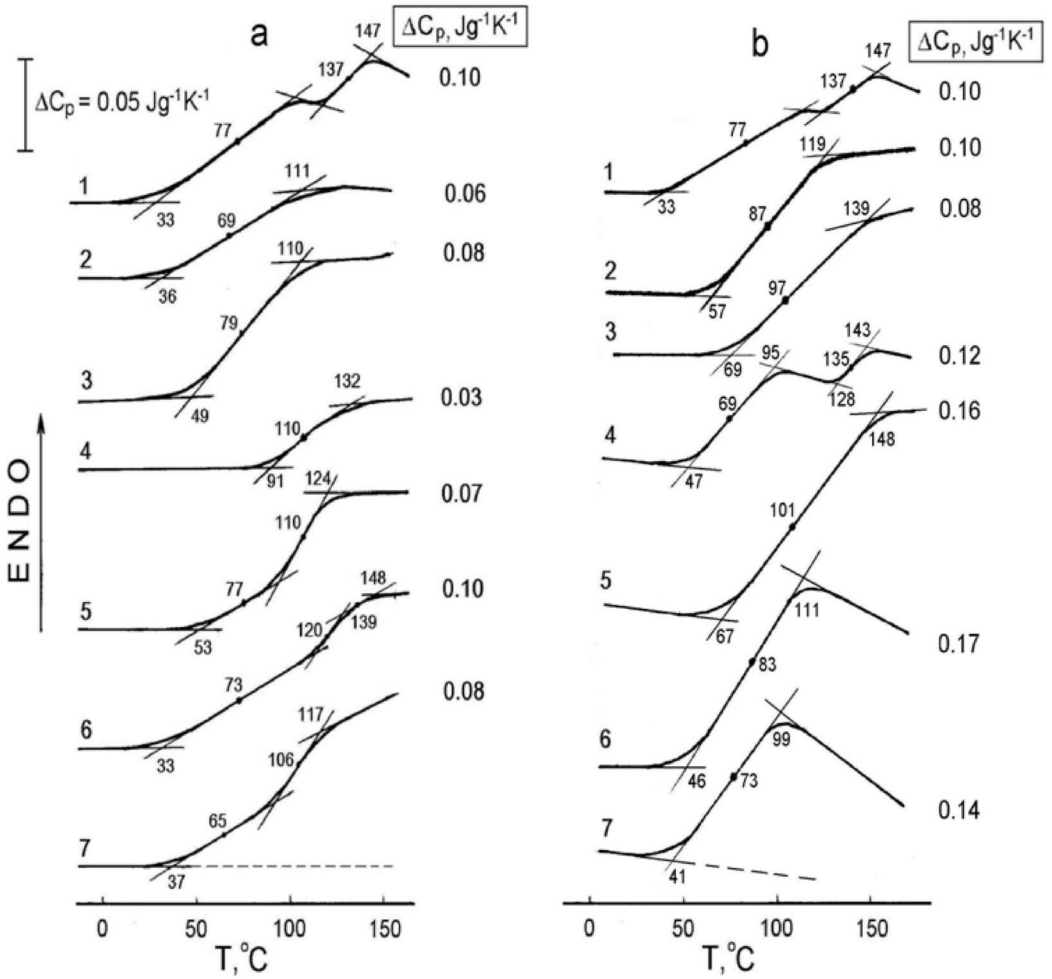

Fig. 5 DSC curves obtained in the region of the PHEMA glass transition for the 83PU–17PHEMA network (1), and for the composites with silica (a) or alumina NPs (b), with 0.25 (2, 4, 6) or 3 wt% oxide (3, 5, 7). Curves 2 and 3 relate to initial, as-prepared oxide particles; curves 4 and 5 to oxide surfaces with MAPS cover, and curves 6 and 7 to oxide surface with APMS groups. The T_g, T_g', T_g'', and ΔC_p values are indicated.

the nanosilica to the PHEMA. As a result, only suppression of the second ΔC_p step (curve 2) or even negligibly small changes in the DSC curve (APMS cover, curve 6) are observed. In contrast, it may be assumed with a high certainty that copolymerisation between the $-CH{=}CH_2$ cover of modified NPs and HEMA occurs, and the covalent bonding of a part of the PHEMA segments with the NP surface takes place. This results in the T_g' displacement from 33 to 91 °C, an increase in T_g from 77 to 110 °C, and a three-fold reduction of the transition width ΔT_g and the ΔC_p step (Fig. 5a, curve 4). A more complicated behaviour of the glass transition, as estimated by DSC, is observed for the nanocomposites with 3 wt% silica (curves 3, 5, and 7). For the alumina-containing nanocomposites, one can see somewhat different DSC results (Fig. 5b). The largest impact of the NPs is attained at 3% of pure alumina (curve 3). Functionalisation of alumina NPs resulted in smaller changes and even in an increase in the ΔC_p step (curves 4–7).

Creep rate spectra

Fig. 6 shows the creep rate (CR) spectra obtained for the 83PU–17PHEMA network and nanocomposites studied in the temperature region from 20 to 160 °C covering the PHEMA glass transition range. The tensile stress of 0.3 MPa was sufficient to obtain the distinct spectra and a satisfactory spectral resolution in this temperature range. The CR spectra of the neat matrix and nanocomposites have complicated contours in the 40–150 °C range including a few partly overlapping peaks, the main one at *ca.* 100 °C (for the neat matrix) and the lesser peaks at 60–80, 90, 110–120, and 140–150 °C. This indicates the multimodal dynamics (strong dynamic heterogeneity) within or close to the PHEMA glass transition in the studied samples.

Generally, the pronounced influence of small oxide additives may be seen, and the spectral contours depend on the type of oxides, their content and the surface structure. The main impact of the NPs is a strong suppression of the segmental dynamics, namely, a sharp decrease in the height of the main CR peak. Secondly, the small CR peak at 140 °C is

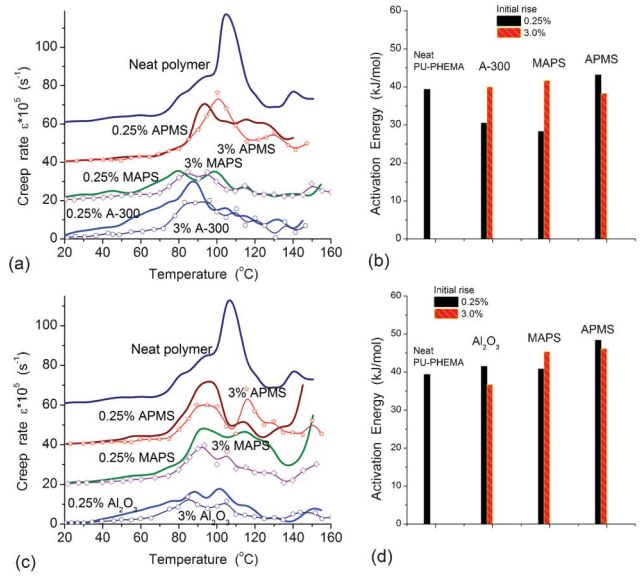

Fig. 6 Creep rate spectra obtained at tensile stress of 0.3 MPa in the temperature region of the PHEMA glass transition for the 83PU–17PHEMA network and nanocomposites based on it, containing 0.25% or 3 wt% of (a) silica and (c) alumina with different surface functional groups; and corresponding activation energies for PU–PHEMA and the nanocomposites with (b) silica and (d) alumina fillers calculated using the initial rise of the creep rate to the first maximum. The creep rate spectra start at about zero creep rate at 20 °C but are displaced by 20 units relative to one another along the ordinate axis.

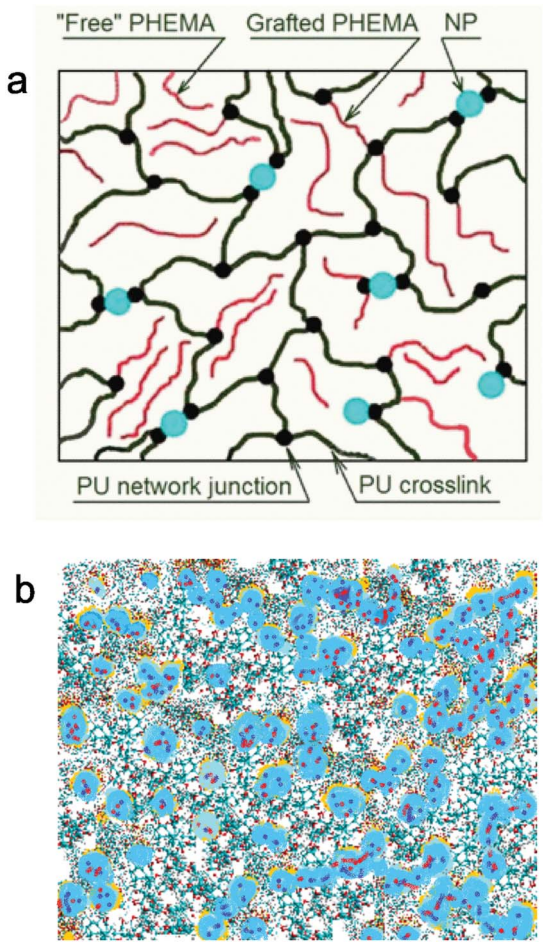

Fig. 7 Schemes showing (a) unusual cross-linked structure in the PU–PHEMA–oxide nanocomposite formed due to the ''double covalent hybridisation'' between residual isocyanate groups of PU and PHEMA, and between the polymer matrix and the NPs; and (b) a composite with a larger content of filler representing aggregates of nanoparticles.

suppressed or displaced to 150 °C in the spectra of the nanocomposites. Thirdly, some increasing creep rates (enhanced mobility) at moderate temperatures of 40–80 °C simultaneously arose for the 0.25 wt% oxides. Finally, similar to the DSC data, the CRS measurements also reveal essential differences in the glass transition dynamics for nanocomposites with different types of functional ''cover'' of the NP surface, that is, a different role of the interfacial dynamics. For the silica-containing composites, the maximum suppression of the dynamics at ~90–160 °C is observed in the case of NPs functionalised by the MAPS groups when the largest displacement of the onset of a sharp acceleration of creep towards higher temperatures occurs. In reality, at 3 wt% silica NPs, a low level of creep rate is retained up to 160 °C (Fig. 6a). Fewer effects are observed in the cases of the untreated silica surface (–OH cover) and, especially, for the NH_2–functionalised surface. In addition, at 0.25 wt% silica NPs some opposite effects of accelerated dynamics (increasing creep rates and a decrease in the activation energy, Fig. 6b) are observed at ~40–80 °C, *i.e.*, in the temperature region between the β- and α-transitions of PHEMA (Fig. 6a). The latter effect is caused, obviously, by some loosening of the molecular packing, with a partial or total collapse, locally, of intermolecular cooperativity of segmental motions in the nanocomposites (''nanoconfined geometries'' effect[2,29]). This leads to a decrease in the activation energy, which is most substantial at the minimum amount of the MAPS–A-300 filler (Fig. 6b). Among the alumina fillers, only untreated alumina (0.25 wt%) gives a slight decrease in the activation energy (Fig. 6d). The difference between the impact of the silica and alumina nanofillers can be explained by a difference in the interactions between the PHEMA and NPs and the matrix molecular packing.

Different CR spectra of the silica-containing nanocomposites, having similar nanostructures (see above) but various NP surface structures, allowed us again to estimate the impact of the PHEMA–silica interfacial interactions on the PHEMA glass transition dynamics in these nanocomposites. In reality, only hydrogen bonds may arise between the PHEMA and the OH ''cover'' or APMS ''cover'' of the silica NPs, whereas stronger covalent PHEMA–silica interfacial bonding may be suggested in the case of MAPS ''cover'' since grafted methacryl groups could copolymerise with HEMA. As a result, the unusual cross-linked structure could be formed in this nanocomposite when ''double hybridisation'', with covalent bonds between PU and PHEMA,[25] and between the polymer matrix and NPs, occurred (see schemes in Fig. 7). Such a composite structure provided, obviously, the largest effect of suppression of segmental dynamics at low NP content (maximum ''constrained dynamics'' effect[2,29]). In contrast, for the alumina-containing composites, the largest effect of constraining dynamics was

attained in the case of the non-treated alumina NP surface, and their special functionalisation reduced this effect (Fig. 6c). In other words, the functionalisation turned out to be useless in the case of using alumina NPs.

In our opinion, this unexpected result can be tentatively explained by two reasons. First, it is in accordance with AFM and DSC data obtained and is associated apparently with a predominant role of an additional complicating nano- and micro-structure of the nanocomposites due to alumina NP functionalisation. Additionally, it should also be taken into account that the non-functionalised surface of crystalline alumina NPs contains mainly γ-phase, that is, both six-fold and four-fold O-coordinated Al atoms; this provides more strong Lewis-Brønsted interactions with polar polymers than in the case of the silica surface.[15]

Modulus *versus* temperature dependencies

Fig. 8 shows the tensile modulus of elasticity E *versus* temperature T plots, as measured from the determination of the deformation by a laser interferometer, for the 83PU–17PHEMA network (E_0) and the silica and alumina-containing nanocomposites (E_n). Generally, one can see a considerable influence of oxide NPs on the course of the $E(T)$ curves. The effects being observed are temperature dependent, and the nanocomposite moduli are typically higher than that for the neat polymer matrix; however, at some temperatures they may be close in magnitude to that of the neat network. On the whole, the E_n/E_0 ratio varies from ~1 to 2.5.

The role of interfacial interactions in the nanocomposites for modulus behaviour may also be seen from Fig. 8a. In the case of CH=CH_2 (MAPS) modified silica NPs, that is, PHEMA–silica covalent bonding, a considerable rise of the E_n/E_0 ratio up to 1.5–2.0 is observed at high temperatures (60–140 °C), with the maximum value at ~120 °C, *i.e.*, in the temperature region of the PHEMA glass transition (curve 5).On the contrary, in the case of NH_2 (APMS) cover of the silica NPs the modulus increased only slightly at high temperatures, whereas E_n/E_0 = 2.0–2.5 at 20 and 60–70 °C (curve 4), that is, at temperatures rather close to the PU glass transition temperatures in this nanocomposite. As was indicated above, that may be readily treated as the consequence of chemical reaction between the very active isocyanate groups of the pristine mixture of reagents and APMS cover that inevitably proceeds during the preparation of the nanocomposite. Due to this reaction, covalent bonding between NPs and the forming PU network occurs promoting an increasing modulus of the nanocomposite at moderate temperatures.

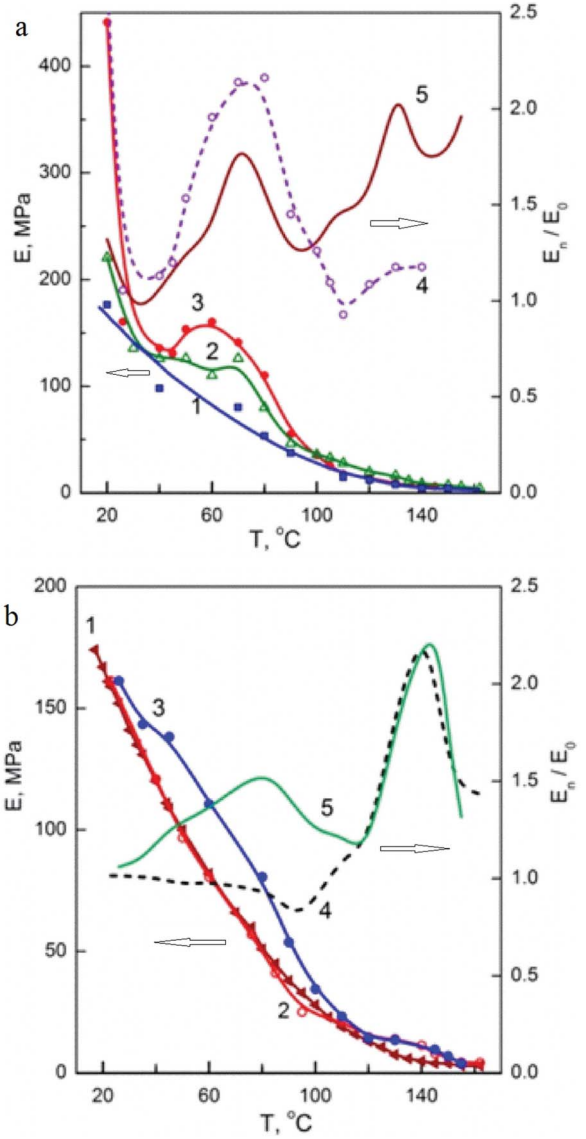

Fig. 8 Modulus of elasticity E *versus* temperature dependencies obtained at a tensile stress of 0.3 MPa for the 83PU–17PHEMA network, E_0 (1), and for the nanocomposites, E_n (2, 3). Lines 4 and 5 indicate the E_n/E_0 ratios. (a) Composites with 3% silica NPs functionalised with APMS (3, 4) or MAPS groups (2, 5). (b) Composites with 0.25% (2, 4) or 3% as-prepared, untreated alumina NPs (3, 5).

Conclusions

Combined AFM/IR/TSDC/DSC/CRS analysis of the structure and dynamics in the PU–PHEMA–oxide nanocomposites with differently functionalised NPs (silica and alumina) was performed over a broad temperature range. Unlike the majority of work on polymer–3D nanoparticle composites, a low content of 3D fumed oxide NPs introduced strongly affected the polymer matrix dynamics and modulus. Thus, the strong suppression of segmental dynamics and two-fold increase in the modulus could be attained at 0.25 wt% oxide NPs. This was caused by the pronounced role of interfacial dynamics due to the creation of unusual cross-linked structures in the nanocomposites, because of the double hybridisation with the formation of covalent bonds between the PU network junctions (residual isocyanate groups) and PHEMA hydroxyls, and between the polymer matrix and the NPs. It was revealed that surface functionalisation of the NPs did not result in substantial positive changes in their dispersion quality (for amorphous silica NPs) but even increased their agglomeration (for crystalline alumina NPs). In general, the impact of the NPs on the PU–PHEMA matrix

properties was controlled by the competitive influence of interfacial interactions and NP dispersion. The first factor was decisive for silica-containing composites where the largest effect was obtained with the MAPS functionalised silica NPs, obviously, due to copolymerisation with HEMA resulting in covalent bonding at the interfaces. On the contrary, for the alumina-containing composites the second factor predetermined the best result obtained with untreated alumina NPs.

Acknowledgements

The work was supported by the FP7-PEOPLE-IRSES project no. 230790, COMPOSITUM.

References

1 (*a*) S. S. Ray and M. Okamoto, *Prog. Polym. Sci.*, 2003, **28**, 1539; (*b*) Y. G. Ke and P. Stroeve, *Polymer-layered silicate and silica nanocomposites*, Elsevier, Amsterdam, 2005; (*c*) M. M. Demir and G. Wegner, *Macromol. Mater. Eng.*, 2012, **297**, 838; (*d*) V. H. Nguyen, Y. Haldorai, Q. L. Pham and J.-J. Shim, *Mater. Sci. Eng., B*, 2011, **176**, 773; (*e*) D.-J. Liaw, K.-L. Wang, Y.-C. Huang, K.-R. Lee, J.-Y. Lai and C.-S. Ha, *Prog. Polym. Sci.*, 2012, **37**, 907; (*f*) D. Wang, X. Huan, L. Zhu, J. Liu, F. Qiu, D. Yan and X. Zhu, *RSC Adv.*, 2012, **2**, 11953; (*g*) S. Peng and B. Bhushan, *RSC Adv.*, 2012, **2**, 8557; (*h*) J. Jiang, Y. Zhang, X. Guo and H. Zhang, *RSC Adv.*, 2012, **2**, 5651; (*i*) A. Pei, J.-M. Malho, J. Ruokolainen, Q. Zhou and L. A. Berglund, Strong nanocomposite reinforcement effects in polyurethane elastomer with low volume fraction of cellulose nanocrystals, *Macromolecules*, 2011, **44**, 4422; (*j*) P. Akcora, H. Liu, S. K. Kumar, J. Moll, Y. Li, B. C. Benicewicz, L. S. Schadler, D. Acehan, A. Z. Panagiotopoulos, V. Pryamitsyn, V. Ganesan, J. Ilavsky, P. Thiyagarajan, R. H. Colby and J. F. Douglas, Anisotropic self-assembly of spherical polymer-grafted nanoparticles, *Nat. Mater.*, 2009, **8**, 354.

2 E. P. Giannelis, R. Krishnamoorti and E. Manias, *Adv. Polym. Sci.*, 1999, **138**, 107.

3 (*a*) M. Moniruzzaman and K. I. Winey, *Macromolecules*, 2006, **39**, 5194; (*b*) V. A. Bershtein, V. M. Gun'ko, L. M. Egorova, Z. Wang, M. Illsley, E. F. Voronin, G. P. Prikhod'ko, P. N. Yakushev, R. Leboda, J. Skubiszewska-Zięba and S. V. Mikhalovsky, *RSC Adv.*, 2012, **2**, 1424.

4 Y. Hu, O. A. Shenderova, Z. Hu, C. W. Padgett and D. W. Brenner, *Rep. Prog. Phys.*, 2006, **69**, 1847.

5 J. L. W. Noell, D. L. Wilkes, D. K. Mohanty and J. E. McGrath, *J. Appl. Polym. Sci.*, 1990, **40**, 1177.

6 D. Tian, P. H. Dubois and K. Jerome, *J. Polym. Sci., Part A: Polym. Chem.*, 1997, **35**, 2295.

7 P. Sysel, R. Pulec and M. Maryska, *Polym. J.*, 1997, **29**, 607.

8 D. A. Suizdak and K. A. Mauritz, *J. Polym. Sci., Part B: Polym. Phys.*, 1999, **37**, 143.

9 (*a*) L. Matejka, K. Dusek, J. Plestil, J. Kriz and L. Lednicky, *Polymer*, 1998, **40**, 171; (*b*) P. Hajji, L. David, J. F. Gerard, J. P. Pascault and G. Vigier, *J. Polym. Sci., Part B: Polym. Phys.*, 1999, **37**, 3172.

10 V. A. Bershtein, L. M. Egorova, P. N. Yakushev, P. Pissis, P. Sysel and L. Brozova, *J. Polym. Sci., Part B: Polym. Phys.*, 2002, **40**, 1056.

11 (*a*) G. Tsagaropoulos and A. Eisenberg, *Macromolecules*, 1995, **28**, 396; (*b*) S. W. Jin, H. Y. Keunok and H. I. Kim, *Polymer*, 2004, **28**, 487; (*c*) J. Berriot, H. Montes, F. Lequeux, D. Long and P. Sotta, *Macromolecules*, 2002, **35**, 9756; (*d*) C. Théneau, S. M. Salmerón, J. C. Rodriguez Hernández, M. Monleón Pradas, J. M. Saiter and J. M. Gómez Ribelles, *Eur. Phys. J. E*, 2007, **24**, 69; (*e*) D. Fradiadakis, P. Pissis and L. Bokobza, *Polymer*, 2005, **46**, 6001; (*f*) V. Arrighi, I. J. McEwen, H. Qian and M. B. Serrano Prieto, *Polymer*, 2003, **44**, 6259; (*g*) A. S. Hoffman, *Adv. Drug Delivery Rev.*, 2012, **64**, 18.

12 (*a*) V. M. Gun'ko, E. F. Voronin, V. I. Zarko, E. V. Goncharuk, V. V. Turov, S. V. Pakhovchishin, E. M. Pakhlov, N. V. Guzenko, R. Leboda, J. Skubiszewska-Zięba, W. Janusz, S. Chibowski, E. Chibowski and A. A. Chuiko, *Colloids Surf., A*, 2004, **233**, 63; (*b*) V. M. Gun'ko, E. F. Voronin, L. V. Nosach, E. M. Pakhlov, N. V. Guzenko, R. Leboda and J. Skubiszewska-Zięba, *Adsorpt. Sci. Technol.*, 2006, **24**, 143; (*c*) V. M. Gun'ko, E. F. Voronin, L. V. Nosach, E. M. Pakhlov, O. E. Voronina, N. V. Guzenko, O. A. Kazakova, R. Leboda and J. Skubiszewska-Zięba, *Appl. Surf. Sci.*, 2006, **253**, 2801; (*d*) V. M. Gun'ko, E. F. Voronin, E. M. Pakhlov, V. I. Zarko, V. V. Turov, N. V. Guzenko, R. Leboda and E. Chibowski, *Colloids Surf., A*, 2000, **166**, 187.

13 (*a*) B. J. Ash, R. W. Siegel and L. S. Schadler, *Macromolecules*, 2004, **37**, 1358; (*b*) S. Zhao, L. S. Schadler, R. Duncan, H. Hillborg and T. Auletta, *Compos. Sci. Technol.*, 2008, **68**, 2965.

14 V. Bershtein, V. Gun'ko, L. Egorova, N. Guzenko, E. Pakhlov, V. Ryzhov and V. Zarko, *Polymer*, 2009, **50**, 860.

15 V. A. Bershtein, V. M. Gun'ko, L. M. Egorova, N. V. Guzenko, E. M. Pakhlov, V. A. Ryzhov and V. I. Zarko, *Langmuir*, 2010, **26**, 10968.

16 (*a*) V. A. Bershtein, L. V. Karabanova, T. E. Sukhanova, P. N. Yakushev, L. M. Egorova, E. D. Lutsyk, A. V. Svyatyna and M. E. Vylegzhanina, *Polymer*, 2008, **49**, 836; (*b*) L. V. Karabanova, V. A. Bershtein, T. E. Sukhanova, P. N. Yakushev, L. M. Egorova, E. D. Lutsyk, A. V. Svyatyna and M. E. Vylegzhanina, *J. Polym. Sci., Part B: Polym. Phys.*, 2008, **46**, 1696; (*c*) T. V. Chirila, K. A. George, W. A. A. Ghafor, S. J. Pas and A. J. Hill, *J. Appl. Polym. Sci.*, 2012, **126**, E455; (*d*) M. Alizadeh, F. Abbasi, M. Farahi and K. Jalili, *J. Appl. Polym. Sci.*, 2012, **124**, 985; (*e*) E. Žagar and M. Žigon, *Prog. Polym. Sci.*, 2011, **36**, 53.

17 V. A. Bershtein, V. M. Gun'ko, L. V. Karabanova, T. E. Sukhanova, P. N. Yakushev, L. M. Egorova, O. B. Glievyy, E. D. Lutsyk, E. M. Pakhlov, A. A. Turova, V. I. Zarko and M. E. Vylegzhanina, *J. Macromol. Sci., Part B: Phys.*, 2010, **49**, 18.

18 (*a*) M. D. Lehah and S. L. Cooper, *Polyurethane in Medicine and Surgery*, CRC Press, Boca Raton, FL, 1986, pp. 158–167; (*b*) D. Li, H. Chen, S. Wang, Z. Wu and J. L. Brash, *Acta Biomater.*, 2011, **7**, 954.

19 (*a*) R. W. Paynter, H. Martz and R. Guidoin, *Biomaterials*, 1987, **8**, 94; (*b*) *Handbook of biopolymers and biodegradable plastics*, ed. S. Ebnesajjad, Elsevier, 2013, DOI: 10.1016/B978-1-4557-2834-3.10002-3.

20 R. J. Thoma and R. E. Phillips, *J. Biomed. Mater. Res.*, 1987, **21**, 525.

21 M. Szycher, in *Blood Compatible Materials and Devices Lancaster*, Technomic Publishing Co., 1991, pp. 33–85.
22 L. V. Karabanova, G. Boiteux, O. Gain, G. Seytre, L. M. Sergeeva and E. D. Lutsyk, *Polym. Int.*, 2004, **53**, 2051.
23 V. V. Shilov, L. V. Karabanova, L. David, G. Boiteux, G. Seytre, Y. P. Gomza, S. D. Nesin, L. M. Sergeeva, E. D. Lutsyk and A. V. Svyatyna, *Polim. Zh.*, 2005, **27**, 255.
24 L. V. Karabanova, G. Boiteux, G. Seytre, I. Stevenson, O. Gain, C. Hakme, L. M. Sergeeva, E. D. Lutsyk and A. Svyatyna, *J. Non-Cryst. Solids*, 2009, **355**, 1453.
25 L. V. Karabanova, L. M. Sergeeva, A. V. Svyatyna, P. N. Yakushev, L. M. Egorova, V. A. Ryzhov and V. A. Bershtein, *J. Polym. Sci., Part B: Polym. Phys.*, 2007, **45**, 963.
26 V. M. Gun'ko, V. I. Zarko, R. Leboda and E. Chibowski, *Adv. Colloid Interface Sci.*, 2001, **91**, 1.
27 V. M. Gun'ko, V. V. Turov, R. Leboda, V. I. Zarko, J. Skubiszewska-Zięba and B. Charmas, *Langmuir*, 2007, **23**, 3184.
28 V. M. Gun'ko, V. I. Zarko, V. V. Turov, O. I. Oranska, E. V. Goncharuk, Y. M. Nychiporuk, E. M. Pakhlov, G. R. Yurchenko, R. Leboda, J. Skubiszewska-Zięba, V. D. Osovskii, Y. G. Ptushinskii, A. G. Derzhypolskyi, D. A. Melenevsky and J. P. Blitz, *Powder Technol.*, 2009, **195**, 245.
29 V. A. Bershtein and P. N. Yakushev, *Adv. Polym. Sci.*, 2010, **230**, 73.
30 V. M. Gun'ko, V. I. Zarko, E. V. Goncharuk, L. S. Andriyko, V. V. Turov, Y. M. Nychiporuk, R. Leboda, J. Skubiszewska-Zięba, A. L. Gabchak, V. D. Osovskii, Y. G. Ptushinskii, G. R. Yurchenko, O. A. Mishchuk, P. P. Gorbik, P. Pissis and J. P. Blitz, *Adv. Colloid Interface Sci.*, 2007, **131**, 1.
31 (*a*) Proceedings of the International Discussion Meeting on Relaxations in Complex Systems, *J. Non-Cryst. Solids*, ed. K. L. Ngai, E. Riande and G. B. Wright, 1994, vol. 172–174; (*b*) V. M. Gun'ko and V. V. Turov, *Nuclear Magnetic Resonance Studies of Interfacial Phenomena*, CRC Press, Taylor & Francis Group, Boca Raton, 2013.
32 (*a*) T. Kanaya, T. Kawaguchi and K. Kaji, *J. Chem. Phys.*, 1996, **105**, 4342; (*b*) R. Zorn, A. Arbe, J. Colmenero, B. Frick, D. Richter and U. Buchenau, *Phys. Rev. E: Stat. Phys., Plasmas, Fluids, Relat. Interdiscip. Top.*, 1995, **52**, 781; (*c*) J. Colmenero, A. Arbe, G. Coddens, B. Frick, C. Mijangos and H. Reinecke, *Phys. Rev. Lett.*, 1997, **78**, 1928; (*d*) U. Buchenau, C. Schönfeld, D. Richter, T. Kanaya, K. Kaji and R. Wehrmann, *Phys. Rev. Lett.*, 1994, **73**, 2344; (*e*) T. Kanaya, T. Ishida, T. Kawaguchi and K. Kaji, *Phys. B*, 1995, **213**(214), 502.
33 V. A. Bershtein and V. A. Ryzhov, *Adv. Polym. Sci.*, 1994, **114**, 43.
34 V. A. Bershtein and V. M. Egorov, *Differential Scanning Calorimetry of Polymers. Physics, Chemistry, Analysis, Technology*, Ellis Horwood, New York, 1994.

